Lawrence Berkeley National Laboratory

Title

Development of Container Free Sample Exposure for Synchrotron X-ray Footprinting

Authors

Gupta, Sayan
Chen, Yan
Petzold, Christopher J
et al.

Development of container free sample exposure for synchrotron X-ray footprinting

Sayan Gupta[1], **Yan Chen**[1], **Christopher J. Petzold**[1], **Daniel P. DePonte**[2], **Corie Y. Ralston**[*,1]

[1]Lawrence Berkeley National Laboratory, Berkeley, California 94720, United States

[2]Stanford Linear Accelerator Center, Menlo Park, California 94025, United States

Abstract

The method of X-ray Footprinting and Mass Spectrometry (XFMS) on large protein assemblies and membrane protein samples requires high flux density to overcome the hydroxyl radical scavenging reactions produced by the buffer constituents and the total protein content. Previously, we successfully developed microsecond XFMS using microfluidic capillary flow and a micro-focused broadband X-ray source at the Advanced Light Source synchrotron beamlines, but the excessive radiation damage incurred when using capillaries prevented the full usage of a high-flux density beam. Here we present another significant advance for the XFMS method: the instrumentation of a liquid injection jet to deliver container free samples to the X-ray beam. Our preliminary experiments with a liquid jet at a bending magnet X-ray beamline demonstrate the feasibility of the approach, and show a significant improvement in the effective dose for both the Alexa fluorescence assay and protein samples compared to conventional capillary flow methods. The combination of precisely controlled high dose delivery, shorter exposure times, and elimination of radiation damage due to capillary effects significantly increases the signal quality of the hydroxyl radical modification products and the dose-response data. This new approach is the first application of container free sample handling for XFMS, and opens up the method for even further advances, such as high-quality microsecond time-resolved XFMS studies.

Graphical Abstract

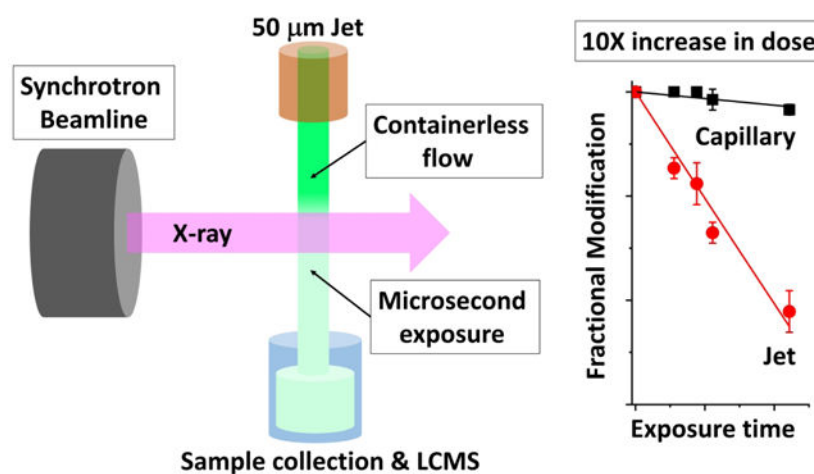[*]**Corresponding Author**: Phone: 510-486-4299. CYRalston@lbl.gov.

The authors declare no competing financial interest.

X-ray Footprinting and Mass Spectrometry (XFMS) is an in situ hydroxyl radical (•OH) labeling method in which broadband synchrotron X-ray irradiation dissociates solvent water to produce hydroxyl radicals, which in turn covalently modify solvent accessible amino acid side chains of proteins[1]. In regions where a protein is folded or bound to a partner, side chains are inaccessible to solvent, and therefore protected from hydroxyl radical labeling. High-resolution liquid chromatography-mass spectrometry is then used to analyze the stable covalent modifications produced, which provides structural information at the single residue level[2, 3]. Ionizing radiation with adequate flux density such as high energy electrons[4] or γ-rays[5] can also be used for hydroxyl labeling of proteins, and hydroxyl labeling of protein side chains can be carried out by non-radiolytic methods. Fenton chemistry, for example, is one of the most common lab-based •OH methods used to determine protein interactions and dynamics[2, 6]. However, chemical production of hydroxyl radicals relies on the addition of reagents such as Fe-EDTA and H_2O_2 which can affect protein conformation, as well as remove essential metal ions necessary for protein function, or can damage/unfold proteins. The UV-laser-induced •OH labeling method known as FPOP[7, 8] is another common method that requires the addition of ~15 mM H_2O_2, which can cause uncontrolled conformational changes or oxidations[4]. Other methods such as high voltage discharge[9] and electrochemical oxidation[10] can be used for protein hydroxyl radical labeling. All the hydroxyl radical generation techniques have their pros and cons depending on the accessibility to the user and biomolecular system under study. However, when hydroxyl radical labeling is combined with other mass spectrometry-based covalent labeling methods such as GEE[11, 12], CF3[13] labeling, or H/D exchange mass spectrometry[14, 15], the number of side chains probed and the information on backbone dynamics is enhanced, all together providing useful and thorough information on protein conformation and interactions in solution[16]. The unique advantages of synchrotron-based XFMS include the following: First, the dose or the amount of •OH labeling can be adjusted from 2 to 10-fold by varying the flow rate of the sample across the X-ray beam. This simple approach generates side chain specific hydroxyl radical reactivity rate constants that can be used for accurate and quantitative comparisons between multiple states of complex biological samples[17]. Second, in situ •OH generation has the advantage of allowing the use of many types of sample buffer conditions. Third, focused synchrotron X-rays provide the ideal energy range (2–10 keV) to penetrate nano to

microliters of the aqueous sample solution yielding •OH labeling in the microsecond range, which is short enough to prevent any severe perturbation to the sample[3]. In addition, radiolytic labeling can probe time-resolved events and locate positions and dynamics of side chain-bound water interactions, which are often critical for protein structure and function, particularly for membrane protein receptors, transporters, and ion channels[18–20]. It has been shown that the higher the dose and the shorter the exposure time, the better the yield of •OH labeling, the lower the secondary damage effects, and the larger the complex that can be studied[21].

In the XFMS method, instrumentation for sample exposure has been continuously evolving towards the more efficient use of high flux density X-ray beams. Installation of a focusing mirror at the broadband bending magnet source beamline X28C at the National Synchrotron Light Source (NSLS) at Brookhaven National Laboratory, for instance, increased the effective flux density on the sample by nearly 10 fold, which enabled the feasibility of the investigation of millisecond time-resolved studies for membrane protein complexes and in-vivo assembly of ribosomal components[18, 22, 23]. Recently, the effective flux density was increased by another 30 fold and the time scale of the method extended to the microsecond regime using a micron-sized focused broadband X-ray beam and a microfluidic capillary flow sample handling system at beamline 5.3.1 at the Advanced Light Source (ALS)[3] and XFP 17BM beamline at the NSLS II, BNL[24]. In addition to this improvement in flux density, there have been other XFMS enabling advances such as those in mass spectrometry resolution and sensitivity, and new analysis approaches which have improved detection of low yield modification products[25]. These developments have resulted in a growing user community with a diverse range of complex biomolecular systems of interest[1, 26]. Nevertheless, a major key challenge remains: the introduction of sufficient hydroxyl radical dose without excessive exposure and loss of data quality.

In this report, we introduce a new high dose sample handling technology for the XFMS experiment using Rayleigh liquid jets. The technology was inspired by recent developments in sample delivery systems employed at X-ray Free-Electron Laser (XFEL) sources to develop a "container free" sample for diffraction studies[27]. The container free sample delivery for XFMS eliminates problems associated with using standard glass capillaries, including excessive heating due to absorption of X-rays by the capillary wall, as well as inhomogeneous flow and clogging issues. Using this technology at an unfocused bending magnet beamline at the ALS, we have shown an increase in the effective dose to the sample by 5 to 10 fold, based on both a fluorophore dye assay and the level of amino acid side chain modification in a protein. In addition, we show that the jet sample delivery method improves the quality of the pseudo-first-order hydroxyl radical reactivity rate, which is a critical factor for quantitative comparisons of solvent accessibility changes. This new method represents a significant advance for the XFMS experiment and confirms that use of jet sample delivery enables microsecond footprinting of small globular protein systems at an unfocused bending magnet broadband X-ray beamline.

Materials and Methods

Sample preparation and exposure-setup

The 5 μM Alexa 488 fluorescence dye (Thermo Fisher Scientific) and 10 mM horse heart cytochrome-c (cyt c) (Sigma) were prepared in 10 mM phosphate buffer. Radiolysis of samples was performed at ALS beamline 3.2.1, which is a broadband bending magnet beamline with beam size fixed at ~10 mm × 100 mm and beam energy of 3 – 12 keV. The microfluidic capillary or the jet nozzle was mounted on a manually adjustable stage capable of horizontal and vertical scans in submillimeter steps. A photodiode was used to detect the beam through a narrow orifice (1 mm diameter) on the sample mount for beam alignment. A 5 mm thick lead (Pb) window of 2 mm (vertical) by 4 mm (horizontal) was placed around the most intense center of the beam. Samples were delivered using either capillaries or liquid jets. For the capillary method, three sizes were used: internal/outer diameter (ID μm/OD μm) of 100/160, 100/360, 200/360 and 50/360 (Molex polymicro products: https://www.molex.com), and samples were flowed past the X-ray beam within the capillaries. For the liquid jet delivery method, jets were created by pushing solution out from the same capillaries, but the samples were exposed at an alternate location, 0.5–1 cm downstream from the end of the polished capillary nozzle (Figure S1). The set-up consisted of a high-pressure syringe pump (Harvard Apparatus) for loading and driving samples using 1 or 2.5 ml gas-tight glass lure-lock syringes (Hamilton), and micro-tight zero dead volume fittings (Idex Health & Science) to mount the capillaries and sample holder such that the sample flowed past the X-ray beam with or without capillary material between the X-rays. For comparison between capillary and jet, samples were exposed under the same flow rate and beam alignment conditions (Table S1). Microscopic image analysis using a strobe light at 500 Hz (MicroFab) and a delay sweep up to 500 microseconds showed a consistent jet profile for up to a distance of 8 mm from the ejection point with a minimum flow speed of 2 and 3 m /s for the 100/360 and 50/360 μm nozzles respectively. The jet nozzle was connected to the syringe pump by 200/360 ID tubing, which provided flexibility in a confined space and also lowered the backpressure. The microfluidic capillary nozzle was mounted within 2 mm above the X-ray window at ALS beamline 3.2.1. The jet nozzle was pushed downward for carrying out the sample exposure inside the polymicro tube. The nozzles were carefully polished to reduce any flow perturbation and ensure jet consistency. The sample exposure either inside the capillary tube or jet was carried out at variable speeds to generate a dose-dependent degradation and yield of modification of Alexa-488 and cyt c. All samples were collected and analyzed as required by fluorescence spectrometry (QuantiFluor ST, Promega) or standard bottom-up LCMS[3]. Sample preparation, exposure, and analysis were done in triplicate.

Mass Spectrometry and Data Analysis

The samples exposed at ALS beamline 3.2.1 were digested using standard methods with trypsin enzyme (Promega) overnight at 37°C at pH 8 in 50 mM ammonium bicarbonate buffer and analyzed on an Agilent 6550 iFunnel Q-TOF mass spectrometer (Agilent Technologies, Santa Clara, CA) coupled to an Agilent 1290 LC system (Agilent) as described previously[3, 14]. The unmodified and modified peptide fragments were identified by a Mascot database search of the tandem mass spectrometry data collected in the data-

dependent mode. The abundance (peak area) of the identified unmodified and modified peptides at each irradiation time point were measured from their respective extracted ion chromatogram of the mass spectrometry data collected in the precursor ion mode using the Agilent Mass Hunter V 2.2 software. The fraction unmodified for each peptide was calculated as the ratio of the integrated peak area of the unmodified peptide to the sum of integrated peak areas from the modified and unmodified peptides. The dose-response curves (fraction unmodified vs. X-ray exposure) were fitted to single exponential functions in Origin® Version 7.5 (OriginLabs). The rate constant, k (sec^{-1}), was used to measure the reactivity of a chain towards hydroxyl radical-induced modification[28].

Results and Discussion

XFMS sample exposure using a micro-focused beam

XFMS is a flux density-driven method. The higher the number of photons per unit area, the shorter the time necessary to generate sufficient side-chain modifications for mass spectrometric detection and analysis[3]. In addition, shorter exposures produce less perturbation to the biomolecular system under study. Therefore, a compact micro-focused high flux density broadband X-ray source is generally ideal for the XFMS experiment. In the current XFMS set-up, protein sample in buffer is passed via a syringe pump through a capillary across the path of the X-ray beam[3]. To expose samples homogenously with a micron-sized focused beam, the internal diameter (ID) of the capillary is matched to the full-width-half-max (FWHM) of the beam. The volumetric flow rate and sample velocity, beam size, and capillary ID determine the exposure time as represented by the equations below.

$$t = \frac{\pi r^2 l}{Q} \tag{1}$$

$$t = \frac{l}{v} \tag{2}$$

Where exposure time, volumetric flow rate, flow velocity, internal radius, and length of the exposed tube are t, Q, v, r and l respectively. These parameters altogether define the XFMS regime (Figure 1 and Figure S2) and determine the feasibility of using capillary flow for protein labeling at high flux density beamlines such as X28C at the NSLS, beamline 5.3.1 at the ALS, and beamline 17BM at the NSLS II, as well as the low flux density ALS beamline 3.2.1, which was used in the current study, to achieve microsecond sample exposures. The variability of v, r, and t at different vertical beam sizes from 200 μm to 2 mm, which are used in the standard XFMS experiments and in our current study are listed in Table S1[3, 17, 24]. The hydroxyl radical reactivity analysis requires a variation of X-ray dose of 5 to 10 fold in the microsecond to millisecond time regime, and this is readily achievable by varying the flow rate or velocity of the sample passing through the beam. Since flow velocity is inversely proportional to the square the radius of the flow path, for a set of flow volumetric rates, focusing the beam and use of a narrow ID flow path can increase the dynamic range of sample exposures or effective dose on the sample significantly. Having a wider set of exposure time points is advantageous because it enables the determination of rate constants

of both low and highly reactive sites from a single experiment. However, a small and very high flux density beam requires fast sample flow speed through a narrower flow path, which can be disadvantageous in terms of sample handling. A flow ID of lower than 50 μm increases the backpressure significantly, which can perturb native protein structure and sample flow consistency[29–31]. The flow speed range in a narrow ID capillary can extend the overall sample exposure or collection time, which increases heat deposition in the sample holder. Taking into account the various parameters in setting up an XFMS capillary flow experiment (Table S1), our survey determined that with the current generation of broadband focused X-ray beamlines, ideally a 100–200 micrometer ID capillary and an exposure speed range of 0.5 – 5 meter / second is the optimal range for sample exposures using the capillary system.

Limitations in the use of capillary flow

Microfluidic capillary flow sample exposure uses polyamide coated fused silica microcapillaries with specified inner and outer diameters, in which the tubing ensures precise control of the speed of the sample during the sample exposure[3, 32]. Despite the simplicity of sample handling conditions, the use of microcapillaries has limitations. With the decrease in tubing internal diameter, the relative absorption path of capillary material increases relative to the absorption path in the sample, and thus the relative dose on the sample decreases; in other words, dose lost to absorption by the capillary goes up substantially. This is due both to the fact that the absorption profile of X-rays by the glass over the wavelengths used in the XFMS experiment is very similar to the absorption by water, and the fact that the capillary wall size does not decrease linearly with total capillary volume (Table S2). For example, fused silica capillaries suitable for X-ray exposure and tested in this study were obtained from Molex® in sizes of inner to outer diameter ratios of 100 μm / 164 or 360 μm, 200 μm / 360 μm, and 50 μm / 360 μm, corresponding to ratios of sample pathlength to glass pathlength of 1.2 or 0.55, 1.1, and 0.3 (assuming X-rays pass through one-half of the capillary wall and then are absorbed by the full sample pathlength) respectively (Figure S3). To characterize the effect of glass absorption we used a standard Alexa 488 fluorescence assay to monitor the dose-response at the various widths of the capillary (Figure 2) and compared these results to the liquid jet sample delivery system as described in the next section. The liquid jet requires high-pressure fittings to withstand the backpressure generated by a high flow rate. The high-pressure fittings only include the standard 360 μm OD microtight adaptors from IDEX®. In our study we avoided low-pressure connectors using sleeves to fit the 164 μm OD capillary, particularly the 50 μm/164, which had severe leakage problems. Alexa mimics the reaction of fully solvent accessible amino acid side chains to hydroxyl radicals, and the Alexa fluorescence assay is a well-established method to empirically estimate the radiolytic dose required to generate a sufficient amount of radiolytic modification to proteins[32]. The linearity of its fluorescence decay in the dose-response reflects a typical pseudo-first-order kinetic response of hydroxyl radical reactivity, and any deviation from the linearity indicates an abnormality in either the sample preparation or the instrument set-up, and results in poor fitting to determine the hydroxyl radical reactivity constant[3, 18, 33]. Greater modification rates for the shorter timepoints in the dose-response profiles were observed with 50/360 and 100/360 μm ID/OD relative to the 200/360 μm ID/OD capillary. Data fitting determined a rate constant higher

than the dose-response with a 200 μm ID capillary with longer exposure (low flow speed, Table S1) and single-shot exposure using a microfuge tube[21, 32], indicating that rate constants obtained using the 200/360 μm ID/OD capillary might also be artificially high. One explanation is that there might be excessive modification at the initial exposure points due to the resistance of the sample flow, which is more pronounced at higher flow velocity and narrow IDs. The resistance of sample flow inside the capillary is due to the viscous drag or friction imposed by the static glass wall on the sample. The length and diameter of the tube contribute to inhomogeneous flow, and while a thorough fluid flow analysis is beyond the scope of our current discussion, we note that the resistance to laminar flow is inversely proportional to the radius of the tube to the fourth power as given by Poiseuille's law for resistance for liquid samples confined to tubes. For the maximum yield of modification and minimum sample perturbation it is important that we use shortest exposure with maximum flux density. This condition requires a micro-focused beam, narrow sample ID and high flow rate or flow velocity. However, it is clearly evident that when narrow flow IDs and high flow velocities are used the inhomogeneous sample flow can affect data fitting and generate inconsistency in the rate constant measurements under the same experimental conditions. The use of smaller IDs is greatly beneficial for handling low abundance samples, which are often more challenging to purify in larger amounts. In some cases, minimizing sample volume is imperative for studies in which multiple samples in gradients of conditions must be analyzed. Thus, for the samples which require higher flux density and cannot be purified in large quantity, the use of 100 μm or less capillary ID becomes a major challenge for sample loading, exposure, and collection. In addition, the capillary introduces local heating effects due to the absorbed heat of the capillary material. In our current configuration for flow-based exposures on the order of 0.2 to 1 milliseconds, the beam impinges on the sample glass container for an average of 5 seconds (Table S1). Damage to the glass is visible as blackened areas where the beam impinges on the glass, indicating sustained heating (Figure S4). During this prolonged and repeated use for sample exposure, the capillaries clog frequently due to sample deposition, indicating that local heat absorbed by the glass material is substantial. Thus, developing a new container free sample delivery method significantly increases the deliverable dose, increases the quality of the dose-response, and further enhances the efficiency of the XFMS method by enabling very small sample volumes, eliminating sample damage incurred by the sustained heating of the capillary material, and eliminating clogging issues common to the examination of cellular and subcellular fractions.

Design of container free sample exposure set-up

The yield of hydroxyl radical following the ionization of pure water by low energy transfer radiation can vary depending on the energy[34, 35]. However, the production of an adequate steady-state concentration of •OH radical useful for protein labeling depends on the ionization density or the flux density of the incident X-ray beam[3]. As shown in Figure 3, in theory, a significant increase in the flux density is possible by removal of the glass entirely, especially at the lower energies. Hydroxyl radical generation is also energy dependent, and previous studies have estimated a 1.5–2 fold decrease in OH radical production at energies below 1keV relative to 10 keV[35]. Given a ~50 fold increase in photon density at 1keV for the container free approach, this would then translate into a ~25 fold increase in OH radical

concentration at that energy. Therefore, we anticipated a significant increase in the effective dose in pure water in the container free approach, and this was borne out empirically. We surveyed container free sample delivery systems, many currently in use at XFEL sources, based on several parameters, including droplet minimum and maximum speed, droplet volume and speed variability, speed control options, dead volume, and modularity (Table S3)[27, 36]. We considered the liquid jet sample delivery technologies that are known to work with dilute solutions of proteins and dilute cell suspensions. In addition to increasing effective dose on the sample, the liquid jet sample exposure method fulfills the main three criteria that are required for designing a robust sample exposure set-up: first, the flow diameter can be controlled by the size of the jet nozzle and can be matched with the FWHM of the X-ray beam; second, the flow speed can be precisely controlled with a pump over a range such that the X-ray exposure can be varied up to 10-fold; third, sample volume and collection time can be easily manipulated giving advantages over other droplet ejection methods.

The simplest liquid jet is the Rayleigh liquid jet, in which pressurized liquid is pushed through a narrow orifice or a nozzle to produce a stream of liquid as wide as that of the jet nozzle or larger[37, 38]. To obtain a continuous jet the liquid velocity must be sufficiently large to ensure that the kinetic energy overcomes the surface energy at the nozzle. The lower critical number for the jet formation is expressed by the Weber number -

$$We_l = \frac{\rho_l \, r \, v^2}{\gamma} > 4, \tag{3}$$

Where liquid density, the radius of the jet nozzle, sample velocity or jet speed, and surface tension are ρ_l, r, v, and γ respectively. On the other hand, if the liquid velocity is too high, the velocity difference between the liquid and the ambient air can break up the jet. The upper critical number for jet formation is expressed by the Weber number in gas -

$$We_g = \frac{\rho_g \, r \, v^2}{\gamma} > 0.2, \tag{4}$$

Where gas density is ρ_g. In our case, ρ_l and ρ_g are approximately equal to the density of water and air, respectively. Given that these are constant, the lower and upper limit of the jetting regime depends on flow velocity, nozzle diameter, and sample viscous properties (Figure 1). The jetting regime requires higher flow speed compared to the current XFMS regime using a microcapillary flow system. Higher flow speed may decrease the exposure time; therefore, if the beam does not have enough flux density a longer path length can be used to get equivalent exposure. The liquid jet delivery method will be highly beneficial for single to double-digit microsecond exposures for a beam size of 100 μm or less where the use of the capillary is impossible because of technical limitations. To obtain a stable liquid jet it is critical to maintain the jetting velocity, solution viscosity, nozzle diameter and physical stability of the jetting environment (shaking and vibration, etc)[38]. The samples are prepared in an aqueous buffer solution, and therefore only the flow velocity and nozzle diameter determine the jetting regime for XFMS studies. It is noteworthy that the

combination of velocity range for a narrow jet and a variable path length of the beam provides a wider range of X-ray doses possible as compared to the capillary method (inset of Figure 1). The following sections describe the use of an unfocused X-ray beam for the development and characterization of a new liquid jet sample exposure method for XFMS.

Figure 4 shows examples of jets that are designed for sample exposure at ALS beamline 3.2.1. We obtained a stable jet for approximately 8 – 10 mm away from the ejection nozzle with a speed range minimum of 2 m/sec for the 100 μm ID and 5 m/sec for the 50 μm ID tubing. The samples were ejected vertically into the beam path and collected in a tube beneath the beam. The maximum speed of both types of jets was limited by the syringe configuration, which operated at a flow speed of 0.4 – 3 ml/min, as well as pump efficiency due to the elevated backpressure at the high flow rate. A speed higher than 3 ml/min can be achieved by using metallic syringes or HPLC displacement pumps, which in turn can provide exposure times on the order of single- to double-digit microseconds for data collection using a high flux density micro-focused beam (Figure 1). In this study, the available speed range in the syringe-pump together with the beam size of 1.5 to 4 mm was sufficient to obtain observable Alexa fluorescence decay using an unfocused bending magnet beamline, enabling comparison with sample exposure using the liquid jet.

Liquid jets increase the dose for Alexa dye and protein

We monitored the degradation of Alexa fluorescence with the progressive decrease in the speed of the jets within the jetting regime, which in turn resulted in a series of exposure times used to quantify the hydroxyl radical reactivity rate (Figure 5). The variations in the observed fractional degradation at each exposure point among multiple repeats of each sample provide information about the quality of the jet. Excessive degradation, which might be due to the jet instability or widening, is observed with the liquid jet at low sample flow speed (such as near and above 0.8 ms exposure for 100 μm jets)[38]. For future experiments, the X-ray exposure path will be moved closer to the jet nozzle to mitigate this effect. However, the data give a significant result for the purpose of the current study: direct pairwise comparison of reactivity rate constants between the samples exposed inside the microfluidic capillaries and their liquid jet counterparts revealed an increase of dose by a factor of 2.5 – 4 fold upon adopting the containerless sample exposure method (Figure 5). In addition, due to the flow inhomogeneity, the dose-response plot using the 50 and 100 μm ID capillaries appeared to lack linearity and showed excessive modification at the initial points compared to the jet counterpart. Given that the reactivity rate for Alexa in a standard 200 μm capillary (presumably homogenous flow) or single-shot sample exposure in the microfuge tube is around 60 s^{-1}, it is arguable that absorption of the glass in the capillary wall decreases the effective dose as high as 10 fold. We used cytochrome c, a small 12kD globular protein, for quantitative analysis of effective dose and LCMS data quality[19], to characterize this difference. The bottom-up mass spectrometry analysis showed >95% sequence coverage and identified several modifications which were reproducible among various samples repeats and exposure conditions (Figure 6 and Table 1). A representative extracted ion chromatogram for the cyt c peptide [40]TGQAPGFTYTDANK[53] showed significant improvement in the signal quality of the +16 Da oxidized products at Y48, F46, T47 and P44 in the jet compared to microfluidic capillary flow (Figure 6). We also observed

differences in the relative levels of site-specific oxidations at different exposure times, as shown by the high-resolution HPLC-MS profile for both the liquid jet and capillary methods. For example, at 200 μs exposure for the jet delivery method (top left and middle panel, Figure 6) the predominant modification was at Y48; however, at 700 μs (bottom left and middle panel, Figure 6) the predominant modification was at P44-F46. These differences are less pronounced in the capillary data, presumably because the signal to noise level is lower in that data. It is possible that the issues associated with the standard capillary flow system such as inhomogeneous flow obscure differences in the modification rates that are now measurable with the jet system. For instance, Y48 may indeed modify faster than P44-F46, but the differences in the rates are averaged with the capillary system in which a fraction of sample remains in the capillary over the course of the experiment due to the viscous drag. The larger dynamic range in exposure time using narrow jets might be very useful in analyzing samples such as G-protein coupled receptors where the reactivity of certain transmembrane residues is very high due to the presence of bound water. Often longer exposure leads to radiation damage and poor quality of the dose-response. Overall, our data show that the sample jet system provides a measurable level of side-chain modification at exposure times as low as 100 μs with an unfocused bending magnet beamline. The difference in the reactivity rates indicates a 5–10 fold increase in the rate of hydroxyl radical reactivity (Table 1). This opens up the opportunity of carrying out single-digit millisecond time-resolved studies on a low flux density beamline as well.

Conclusion and future directions

We have successfully demonstrated an increase in effective dose for protein samples using an unfocused bending magnet beamline. The sample jets required for XFMS were characterized with Alexa and the small globular protein cyt c. The new sample jet system has improved sample irradiation conditions, eliminated the loss of dose due to the absorption by the glass wall of the capillary, showed a 10 fold increase in effective dose, and increased linearity in the dose-response with no direct heat damage to the samples. The increase in the dose enables shorter exposure times, which decreases the secondary damage to proteins as well as increasing the sensitivity of the technique. The sample jet system will next be tested at the high flux density microfocused beamline NSLS II 17-BM, where we expect to increase the dynamic range of the variation of dose another 5 – 10 fold. The set-up will later be used for more challenging systems, such as in vivo cell studies, large complexes, and membrane proteins, as well as micro-second time resolved in situ hydroxyl labeling studies. Currently, the development of a micro-focus capability at the ALS at beamline 3.3.1 is in progress[39]. This beamline will host the only dedicated XFMS program on the West Coast. Beamline 3.3.1 is located on a white light bend magnet source with an acceptance of 6.2 X 2 mrad, and a planned Pt-coated toroidal focusing mirror centered at 11.1m (2/3 of the distance) from the source. The beamline will deliver 10^{16} photons/sec (energy range of 2 – 10 keV) into a ~ 80 X 80 μm spot size with a power density of >2000W mm^2. We anticipate that the focusable beam along with the use of 20–50 μm jet sample delivery will increase the usable flux density at the sample by > 100 fold compared to the current unfocused beam at ALS 3.2.1 and will advance the exposure limit to single-digit microseconds. Future plans include the design of a mixing jet for high dose microsecond time-resolved XFMS. This development promises to provide novel insights into the structure and dynamics of complex

macromolecules in solution. A more complex jet, the gas dynamics virtual nozzle (GDVN), which uses a pressurized gas stream to focus the liquid jet from the exit nozzle, can be used for producing continuous sample delivery similar to liquid jets but with more advanced control of sample volume, speed, size, and mixing[40–42]. Overall, Rayleigh liquid jets and/or GDVN provide a wide range of jet diameter and speeds and can provide direct on-demand control of speed, size, and mixing which are key for steady-state and time-resolved XFMS studies.

Supplementary Material

Refer to Web version on PubMed Central for supplementary material.

ACKNOWLEDGMENTS

REFERENCES

1. Gupta S; Feng J; Chan LJ; Petzold CJ; Ralston CY, Synchrotron X-ray footprinting as a method to visualize water in proteins. J Synchrotron Radiat 2016, 23 (Pt 5), 1056–69. [PubMed: 27577756]

2. Xu G; Chance MR, Hydroxyl radical-mediated modification of proteins as probes for structural proteomics. Chemical reviews 2007, 107 (8), 3514–43. [PubMed: 17683160]

3. Gupta S; Celestre R; Petzold CJ; Chance MR; Ralston C, Development of a microsecond X-ray protein footprinting facility at the Advanced Light Source. J Synchrotron Radiat 2014, 21 (Pt 4), 690–9. [PubMed: 24971962]

4. Watson C; Janik I; Zhuang T; Charvatova O; Woods RJ; Sharp JS, Pulsed electron beam water radiolysis for submicrosecond hydroxyl radical protein footprinting. Analytical chemistry 2009, 81 (7), 2496–505. [PubMed: 19265387]

5. Ottinger LM; Tullius TD, High-resolution in vivo footprinting of a protein-DNA complex using gamma-radiation. J Am Chem Soc 2000, 122 (24), 5901–5902.

6. Tullius TD; Dombroski BA, Iron(II) EDTA used to measure the helical twist along any DNA molecule. Science 1985, 230 (4726), 679–81. [PubMed: 2996145]

7. Aye TT; Low TY; Sze SK, Nanosecond laser-induced photochemical oxidation method for protein surface mapping with mass spectrometry. Analytical chemistry 2005, 77 (18), 5814–22. [PubMed: 16159110]

8. Hambly DM; Gross ML, Laser flash photolysis of hydrogen peroxide to oxidize protein solvent-accessible residues on the microsecond timescale. Journal of the American Society for Mass Spectrometry 2005, 16 (12), 2057–63. [PubMed: 16263307]

9. Wong JWH; Maleknia SD; Downard KM, Hydroxyl radical probe of the calmodulin-melittin complex interface by electrospray ionization mass spectrometry. J Am Soc Mass Spectr 2005, 16 (2), 225–233.

10. McClintock C; Kertesz V; Hettich RL, Development of an electrochemical oxidation method for probing higher order protein structure with mass spectrometry. Analytical Chemistry 2008, 80 (9), 3304–3317. [PubMed: 18351783]

11. Deperalta G; Alvarez M; Bechtel C; Dong K; McDonald R; Ling V, Structural analysis of a therapeutic monoclonal antibody dimer by hydroxyl radical footprinting. MAbs 2013, 5 (1), 86–101. [PubMed: 23247543]

12. Kaur P; Tomechko SE; Kiselar J; Shi W; Deperalta G; Wecksler AT; Gokulrangan G; Ling V; Chance MR, Characterizing monoclonal antibody structure by carboxyl group footprinting. MAbs 2015, 7 (3), 540–52. [PubMed: 25933350]

13. Cheng M; Zhang B; Cui W; Gross ML, Laser-Initiated Radical Trifluoromethylation of Peptides and Proteins: Application to Mass-Spectrometry-Based Protein Footprinting. Angew Chem Int Ed Engl 2017, 56 (45), 14007–14010. [PubMed: 28901679]

14. Gupta S; Guttman M; Leverenz RL; Zhumadilova K; Pawlowski EG; Petzold CJ; Lee KK; Ralston CY; Kerfeld CA, Local and global structural drivers for the photoactivation of the orange carotenoid protein. Proceedings of the National Academy of Sciences of the United States of America 2015, 112 (41), E5567–74.

15. Orban T; Jastrzebska B; Gupta S; Wang B; Miyagi M; Chance MR; Palczewski K, Conformational dynamics of activation for the pentameric complex of dimeric G protein-coupled receptor and heterotrimeric G protein. Structure 2012, 20 (5), 826–40. [PubMed: 22579250]

16. Limpikirati P; Liu T; Vachet RW, Covalent labeling-mass spectrometry with non-specific reagents for studying protein structure and interactions. Methods 2018, 144, 79–93. [PubMed: 29630925]

17. Gupta S; Shutter M; Remesh SG; Dominguez-Martin MA; Bao H; Feng XA; Chan LJ; Petzold CJ; Kerfeld CA; Ralston CY, X-ray radiolytic labeling reveals the molecular basis of orange carotenoid protein photoprotection and its interactions with fluorescence recovery protein. Journal of Biological Chemistry 2019, Inpress.

18. Gupta S; Chai J; Cheng J; D'Mello R; Chance MR; Fu D, Visualizing the kinetic power stroke that drives proton-coupled zinc(II) transport. Nature 2014, 512 (7512), 101–4. [PubMed: 25043033]

19. Gupta S; D'Mello R; Chance MR, Structure and dynamics of protein waters revealed by radiolysis and mass spectrometry. Proceedings of the National Academy of Sciences of the United States of America 2012, 109 (37), 14882–7.

20. Angel TE; Chance MR; Palczewski K, Conserved waters mediate structural and functional activation of family A (rhodopsin-like) G protein-coupled receptors. Proceedings of the National Academy of Sciences of the United States of America 2009, 106 (21), 8555–60.

21. Bohon J; D'Mello R; Ralston CY; Gupta S; Chance MR, Synchrotron X-ray Footprinting on Tour. 2013.

22. Sullivan MR; Rekhi S; Bohon J; Gupta S; Abel D; Toomey J; Chance MR, Installation and testing of a focusing mirror at beamline X28C for high flux x-ray radiolysis of biological macromolecules. The Review of scientific instruments 2008, 79 (2 Pt 1), 025101. [PubMed: 18315323]

23. Clatterbuck Soper SF; Dator RP; Limbach PA; Woodson SA, In vivo X-ray footprinting of pre-30S ribosomes reveals chaperone-dependent remodeling of late assembly intermediates. Mol Cell 2013, 52 (4), 506–16. [PubMed: 24207057]

24. Asuru A; Farquhar ER; Sullivan M; Abel D; Toomey J; Chance MR; Bohon J, The XFP (17-BM) Beamline for X-ray Footprinting at NSLS-II. J Synchrotron Radiat 2019, In press.

25. Kaur P; Kiselar J; Yang S; Chance MR, Quantitative protein topography analysis and high-resolution structure prediction using hydroxyl radical labeling and tandem-ion mass spectrometry (MS). Molecular & cellular proteomics : MCP 2015, 14 (4), 1159–68. [PubMed: 25687570]

26. Kiselar J; Chance MR, High-Resolution Hydroxyl Radical Protein Footprinting: Biophysics Tool for Drug Discovery. Annu Rev Biophys 2018.

27. Weierstall U, Liquid sample delivery techniques for serial femtosecond crystallography. Philos Trans R Soc Lond B Biol Sci 2014, 369 (1647), 20130337. [PubMed: 24914163]

28. Kiselar JG; Maleknia SD; Sullivan M; Downard KM; Chance MR, Hydroxyl radical probe of protein surfaces using synchrotron X-ray radiolysis and mass spectrometry. Int J Radiat Biol 2002, 78 (2), 101–14. [PubMed: 11779360]

29. Mozhaev VV; Heremans K; Frank J; Masson P; Balny C, High pressure effects on protein structure and function. Proteins 1996, 24 (1), 81–91. [PubMed: 8628735]

30. Brandts JF; Oliveira RJ; Westort C, Thermodynamics of protein denaturation. Effect of pressu on the denaturation of ribonuclease A. Biochemistry 1970, 9 (4), 1038–47. [PubMed: 5417389]

31. Ledward DA, Effects of pressure on protein structure. High Pressure Res 2000, 19 (1–6), 391–400.

32. Gupta S; Sullivan M; Toomey J; Kiselar J; Chance MR, The Beamline X28C of the Center for Synchrotron Biosciences: a national resource for biomolecular structure and dynamics experiments using synchrotron footprinting. J Synchrotron Radiat 2007, 14 (Pt 3), 233–43. [PubMed: 17435298]

33. Angel TE; Gupta S; Jastrzebska B; Palczewski K; Chance MR, Structural waters define a functional channel mediating activation of the GPCR, rhodopsin. Proceedings of the National Academy of Sciences of the United States of America 2009, 106 (34), 14367–72.

34. Fulford J; Bonner P; Goodhead DT; Hill MA; O'Neill P, Experimental determination of the dependence of OH radical yield on photon energy: A comparison with theoretical simulations. J Phys Chem A 1999, 103 (51), 11345–11349.

35. Yamaguchi H; Uchihori Y; Yasuda N; Takada M; Kitamura H, Estimation of yields of OH radicals in water irradiated by ionizing radiation. J Radiat Res 2005, 46 (3), 333–341. [PubMed: 16210790]

36. Roessler CG; Agarwal R; Allaire M; Alonso-Mori R; Andi B; Bachega JF; Bommer M; Brewster AS; Browne MC; Chatterjee R; Cho E; Cohen AE; Cowan M; Datwani S; Davidson VL; Defever J; Eaton B; Ellson R; Feng Y; Ghislain LP; Glownia JM; Han G; Hattne J; Hellmich J; Heroux A; Ibrahim M; Kern J; Kuczewski A; Lemke HT; Liu P; Majlof L; McClintock WM; Myers S; Nelsen S; Olechno J; Orville AM; Sauter NK; Soares AS; Soltis SM; Song H; Stearns RG; Tran R; Tsai Y; Uervirojnangkoorn M; Wilmot CM; Yachandra V; Yano J; Yukl ET; Zhu D; Zouni A, Acoustic Injectors for Drop-On-Demand Serial Femtosecond Crystallography. Structure 2016, 24 (4), 631–40. [PubMed: 26996959]

37. Eggers J; Villermaux E, Physics of liquid jets. Rep Prog Phys 2008, 71 (3).

38. van Hoeve W; Gekle S; Snoeijer JH; Versluis M; Brenner MP; Lohse D, Breakup of diminutive Rayleigh jets. Phys Fluids 2010, 22 (12).

39. Morton SA; Gupta S; Petzold CJ; Ralston CY, Recent Advances in X-Ray Hydroxyl Radical Footprinting at the Advanced Light Source Synchrotron. Protein Pept Lett 2019, 26 (1), 70–75. [PubMed: 30484401]

40. Calvey GD; Katz AM; Schaffer CB; Pollack L, Mixing injector enables time-resolved crystallography with high hit rate at X-ray free electron lasers. Struct Dynam-Us 2016, 3 (5).

41. DePonte DP; Weierstall U; Schmidt K; Warner J; Starodub D; Spence JCH; Doak RB, Gas dynamic virtual nozzle for generation of microscopic droplet streams. J Phys D Appl Phys 2008, 41 (19).

42. Nelson G; Kirian RA; Weierstall U; Zatsepin NA; Farago T; Baumbach T; Wilde F; Niesler FBP; Zimmer B; Ishigami I; Hikita M; Bajt S; Yeh SR; Rousseau DL; Chapman HN; Spence JCH; Heymann M, Three-dimensional-printed gas dynamic virtual nozzles for x-ray laser sample delivery. Opt Express 2016, 24 (11), 1515–1530.
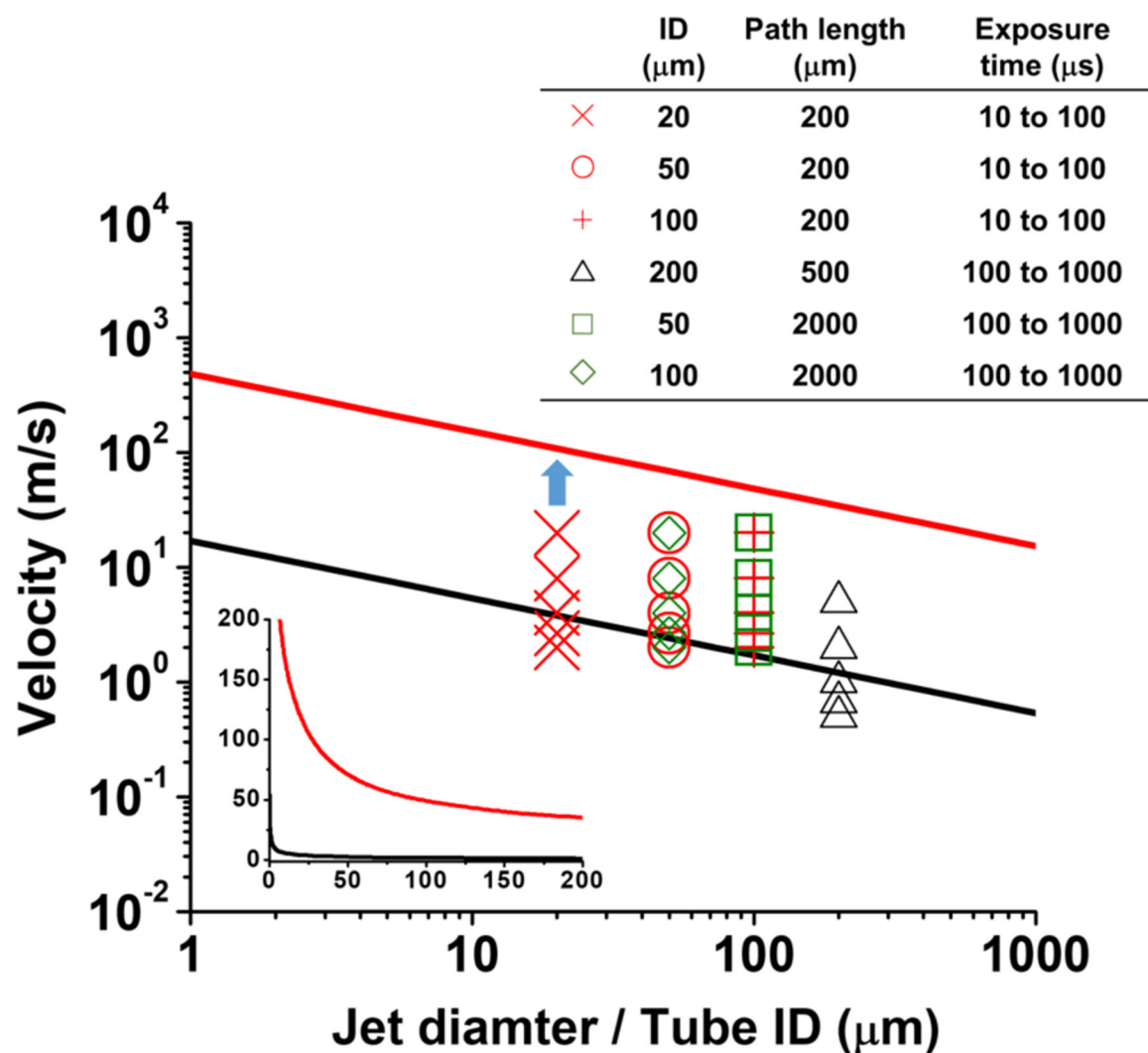
Figure 1.
The XFMS jetting regime is defined by flow velocity, exposure time, and area of exposure. Jetting regime is shown within the lower (black) and upper (red) limit of flow velocity determined from the Weber number (Equations 3 and 4) as a function of jet diameter. The individual points represent the optimum range of velocities for a given sample diameter and beam size for sample exposure. The green set of points indicate the flow velocity selected for the current study at the unfocused beamline. The black set of points were those used in actual XFMS experiments at the ALS and NSLS II using high-flux density focused X-ray beamlines. The red set of points are the estimated range, based on Alexa dose response and protein side chain modification, used for the development of microsecond XFMS at the ALS. Blue arrow indicates a region of higher flow velocity that will provide shorter exposure, which will be useful to minimize sample damage as well as effectively use the higher flux density at a micro-focused beamline. The inset is the jetting regime plotted in linear scale in order to better show that a much wider choice of flow velocity is available with narrower jets.
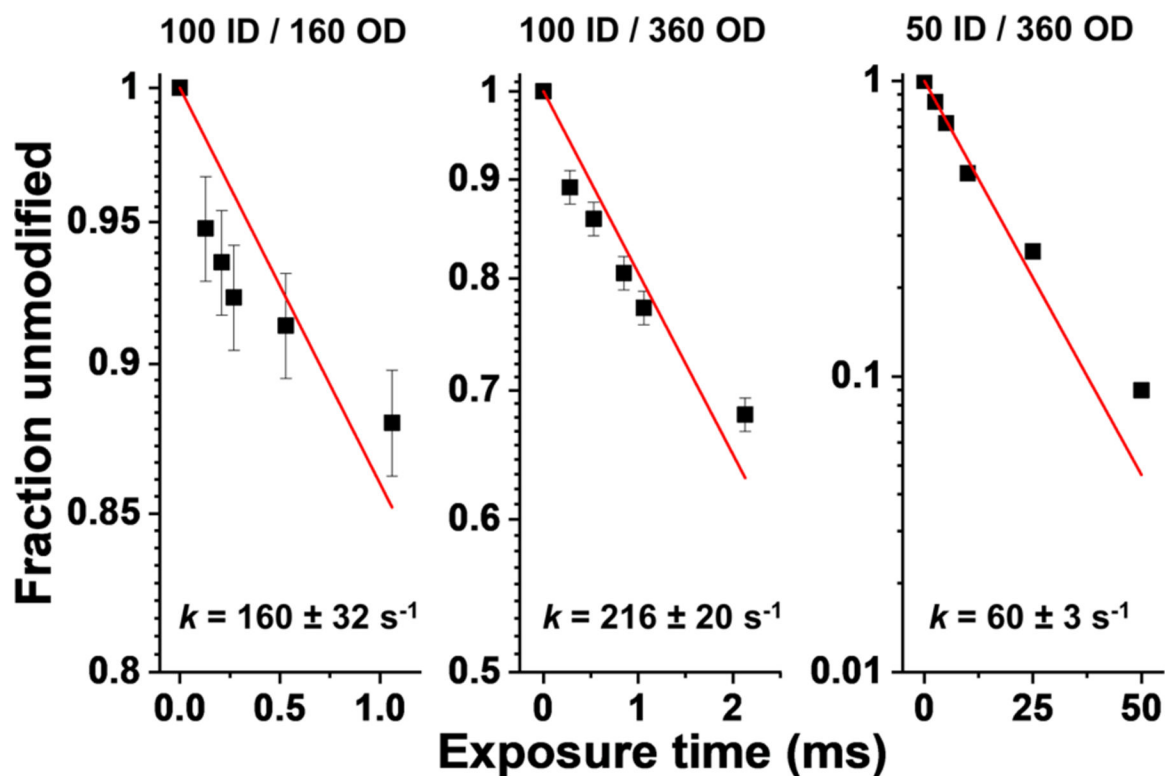
Figure 2.
Dose-response plot consisting of microsecond to millisecond irradiation of 10 μM Alexa in 10 mM phosphate buffer (pH 7) using various ID capillary flow exposures. The length of the X-ray window was set to 2 mm for 50 μm, 100 μm, and 200 μm ID capillary flow to obtain the range of exposure times as indicated in Table S1. The solid red line represents a single exponential fit and rate constants are shown. Individual points represent the mean of three independent measurements with standard error. R-squared values for the fit as calculated via Origin® Version 7.5 are 0.44, 0.88, and 0.99 for the left, middle and right plots, respectively. The flow velocity inside the 50 μm and 100 μm tubing are within the jetting regime and up to 100 fold faster than that of the flow velocity inside the 200 μm tubing used for the standard capillary flow method at the unfocused X-ray beamline. (Table S1)
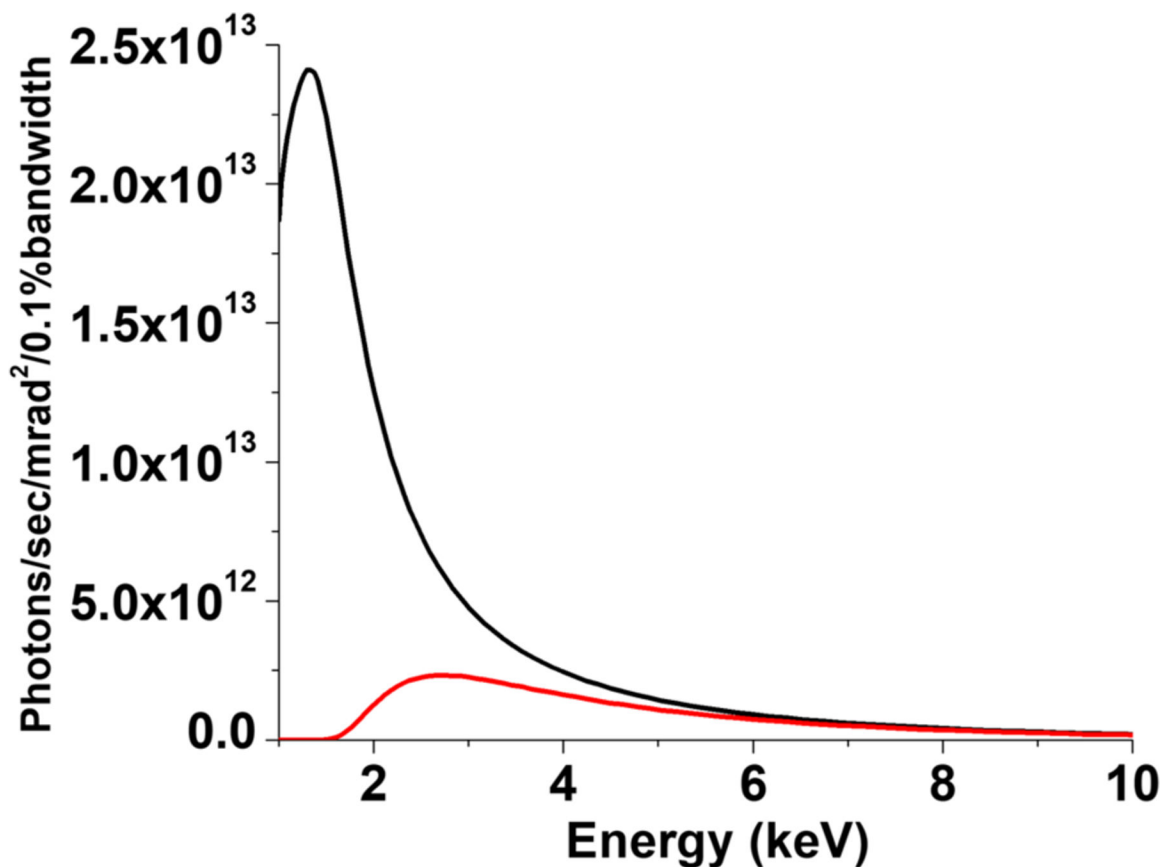
Figure 3.
Removal of glass increases photon absorption by the sample. Calculation of photon spectrum for a sample path-length of 50 μm through a 180 μm glass capillary wall (red) and no glass capillary (black), which corresponds to 50 μm ID – 360 μm OD capillary-flow set-up and 50 μm ID liquid jet set-up respectively. Integration of the plots show >5 fold increase in integrated flux by removing the glass wall. A 1 cm path-length in the air was assumed prior to sample exposure. The calculation used an ALS bend magnet spectrum and transmission/absorption coefficients as given by the Center for X-Ray Optics website (cxro.lbl.gov) calculator. In the case of a 20 μm droplet with and without an 80 μm glass wall, total integrated photons are 10-fold higher than with glass.
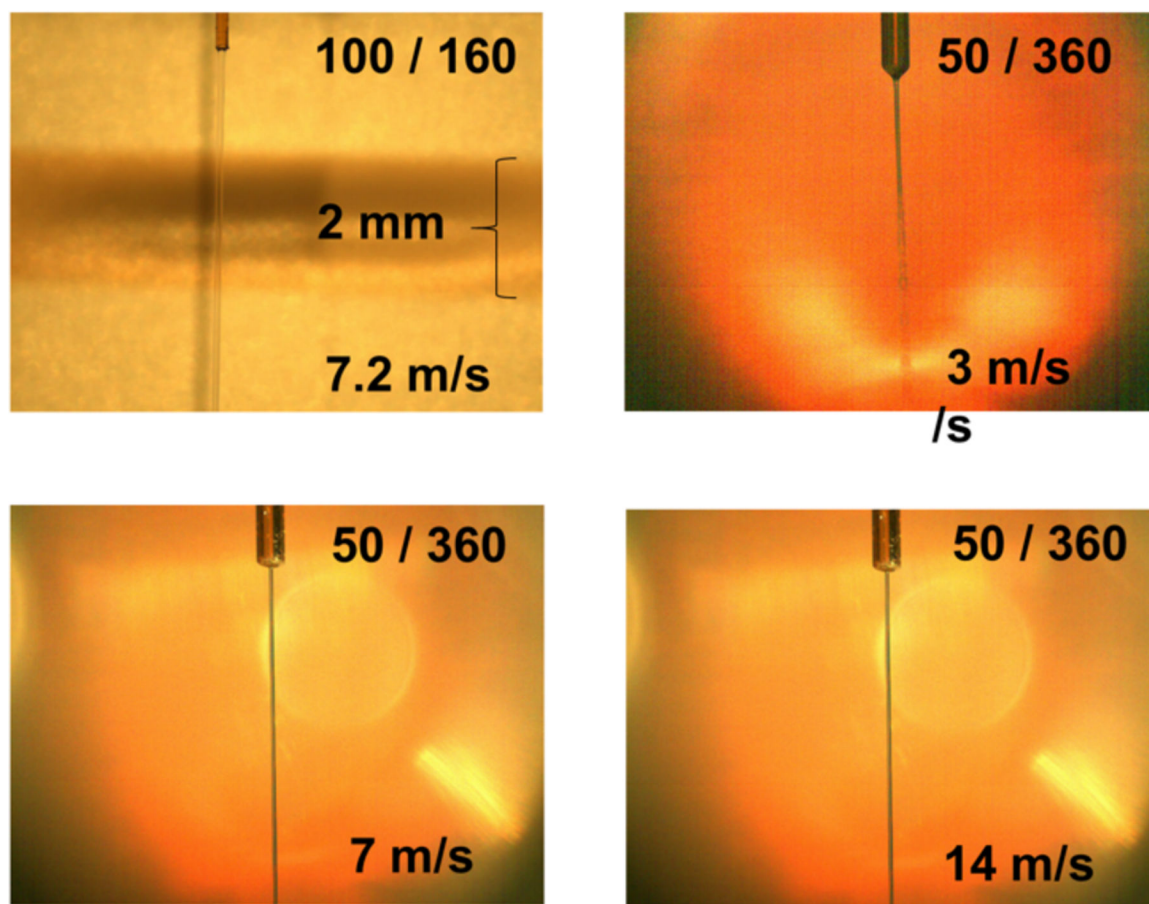
Figure 4.
Snapshots of Rayleigh liquid jets for XFMS. The impression of X-ray beam of vertical length ~ 2mm is show with the 100 μm ID jet (top left panel). A sample flow velocity lower than in the jetting regime produces unstable jets with breakups (top right panel). Stable jets were seen to travel more than 10 cm distance vertically.
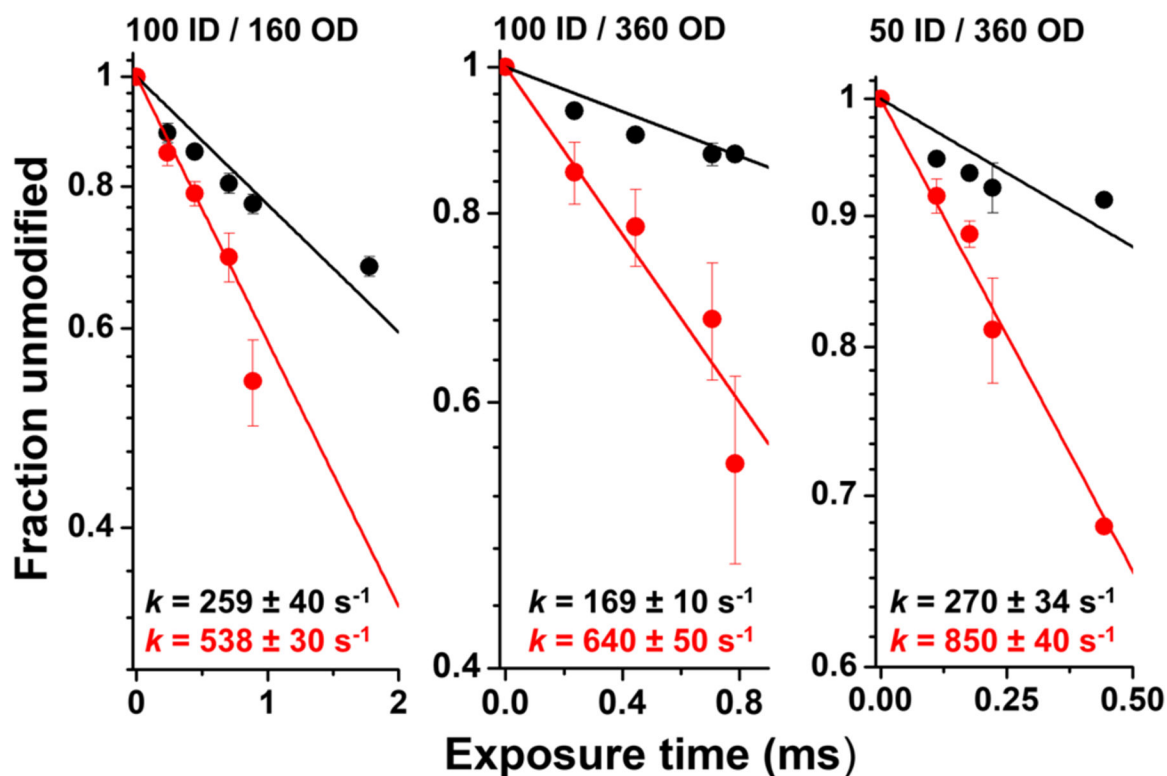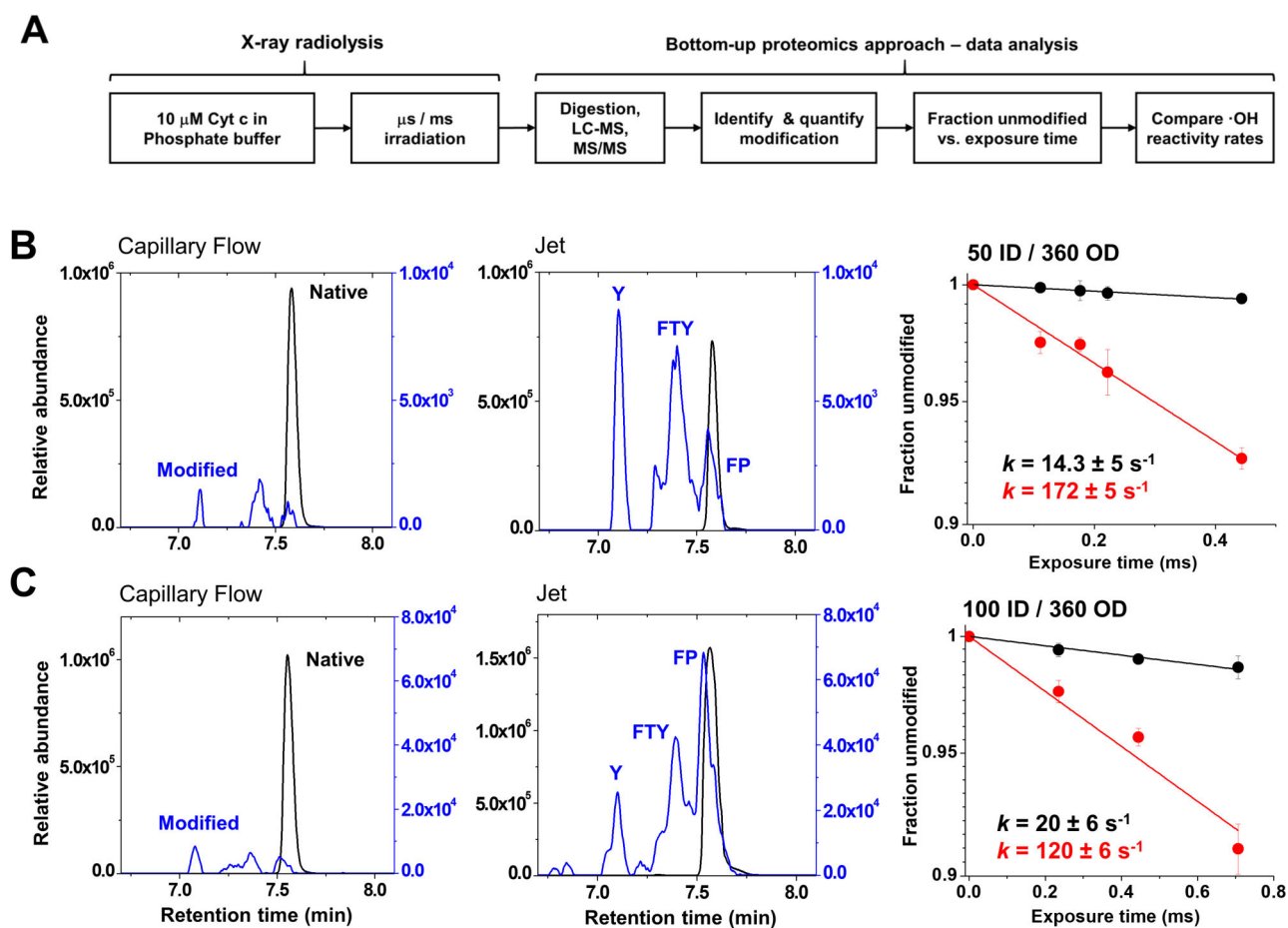
Figure 5.
Liquid jet results in a higher dose in the Alexa assay. Dose-response plot consisting of microsecond irradiation of 10 μM Alexa in 10 mM phosphate buffer (pH 7) using microfluidic capillary flow (black) and liquid jet (red) exposure set-up at high flow rates in the jetting regime. The length of the X-ray window was 2 mm and two types of tube ID were used as indicated. The solid line represents a single exponential fit to initial data points and determines the rate constant (k s $^{-1}$), with individual points representing the mean of three independent measurements with standard error. R-squared values for the fit as calculated via Origin® Version 7.5 are 0.88, 0.91 and 0.59 (from left to right panel) and 0.96, 0.94, and 0.98 for the capillary and jet respectively.

Figure 6.
Liquid jet and capillary flow comparison. (A) Experimental scheme. (B) and (C) The left and middle panel show the extracted ion chromatogram of the doubly protonated native (black), and the doubly protonated +16 Da modified products (blue) of the cyt c peptide [40]TGQAPGFTYTDANK[53]. The modification products eluted as three peaks between 7 and 7.7 min and are shown for the exposed sample at 200 μs using capillary flow or jet with tube ID/OD of 50/360 (B) and 700 μs with tube ID/OD of 100/360 (C).**Figure 6.** The right panels show the fraction of unmodified peptide, which is calculated as the unmodified peak area divided by the sum of unmodified and modified peak areas at a given exposure. The solid line represents a single exponential fit to determine the hydroxyl radical reactivity k (s $^{-1}$), with individual points representing the mean of three independent measurements with standard deviation, for both jet (red) and capillary (black) data. R-squared values for the fit as calculated via Origin® Version 7.5 are between 0.97 and 0.99 for all fits. The site of modification at Y48, F46, T47, and P44 were identified by MS/MS according to the standard MS/MS m/z assignment method (Figure S5)[3, 19].

Table 1:

Comparison of rate constants of hydroxyl radical modifications for cyt c exposed to X-rays using 50 μm liquid jet and 50 μm ID / 360 μm OD microcapillary flow

Sequence of the trypsin fragments[a]	Sites of modification[b]	Hydroxyl radical reactivity rate k (s-1)[c]		Ratio k_{jet}/k_{flow}
		Liquid Jet	Capillary Flow	
9IFVQK13	All residues	8.4 ± 0.8	0.0	∞
28TGPNLHGLFGR38	P30, H33, F36, R38	34.4 ± 1.6	3.0 ± 1.6	11.4
40TGQAPGFTYTDANK53	P44, F46, T47, Y48	172.3 ± 5.1	14.3 ± 6.0	12.4
56GITWK60	I57, W59, K60	282.0 ± 20.1	24.3 ± 11.3	11.8
61EETLMEYLENPK72	E61,E62,M65,Y67,P71	256.4 ± 19.5	80.0 ± 11.0	3.2
80MIFAGIK86	M80, F82, K86	1095.9 ± 102.0	171.2 ± 74.9	10.7
92EDLIAYLK99	K99	51.3 ± 2.1	3.2 ± 2.1	16.0

[a] sequences of tryptic fragments

[b] modified residues, which were identified and confirmed by LCMS as previously described[19]

[c] hydroxyl radical rate constants were estimated by employing a first order exponential fit of the dose-response plot of overall peptide modification as described in experimental procedures and Figure S6. The modified peptide fragments were eluted as a single peak or multiple peaks. The modified peak areas were extracted individually but summed together to calculate the total modification of the respective peptide using methods as previously described[3].